Published OnlineFirst August 7, 2018; DOI: 10.1158/2326-6066.CIR-18-0077

Research Article

Cancer Immunology Research

BET Bromodomain Inhibition Cooperates with PD-1 Blockade to Facilitate Antitumor Response in *Kras*-Mutant Non–Small Cell Lung Cancer

Dennis O. Adeegbe[1], Shengwu Liu[2,3], Maureen M. Hattersley[4], Michaela Bowden[2], Chensheng W. Zhou[2], Shuai Li[2,5], Raven Vlahos[2], Michael Grondine[4], Igor Dolgalev[6], Elena V. Ivanova[2,7], Max M. Quinn[2], Peng Gao[2], Peter S. Hammerman[8], James E. Bradner[8], J. Alan Diehl[9], Anil K. Rustgi[10], Adam J. Bass[2], Aristotelis Tsirigos[6], Gordon J. Freeman[2], Huawei Chen[4], and Kwok-Kin Wong[1]

Abstract

KRAS mutation is present in approximately 30% of human lung adenocarcinomas. Although recent advances in targeted therapy have shown great promise, effective targeting of KRAS remains elusive, and concurrent alterations in tumor suppressors render *KRAS*-mutant tumors even more resistant to existing therapies. Contributing to the refractoriness of *KRAS*-mutant tumors are immunosuppressive mechanisms, such as increased presence of suppressive regulatory T cells (Treg) in tumors and elevated expression of the inhibitory receptor PD-1 on tumor-infiltrating T cells. Treatment with BET bromodomain inhibitors is beneficial for hematologic malignancies, and they have Treg-disruptive effects in a non–small cell lung cancer (NSCLC) model. Targeting PD-1–inhibitory signals through PD-1 antibody blockade also has substantial therapeutic impact in lung cancer, although these outcomes are limited to a minority of patients. We hypothesized that the BET bromodomain inhibitor JQ1 would synergize with PD-1 blockade to promote a robust antitumor response in lung cancer. In the present study, using $Kras^{+/LSL\text{-}G12D}$; $Trp53^{L/L}$ (KP) mouse models of NSCLC, we identified cooperative effects between JQ1 and PD-1 antibody. The numbers of tumor-infiltrating Tregs were reduced and activation of tumor-infiltrating T cells, which had a T-helper type 1 (Th1) cytokine profile, was enhanced, underlying their improved effector function. Furthermore, lung tumor–bearing mice treated with this combination showed robust and long-lasting antitumor responses compared with either agent alone, culminating in substantial improvement in the overall survival of treated mice. Thus, combining BET bromodomain inhibition with immune checkpoint blockade offers a promising therapeutic approach for solid malignancies such as lung adenocarcinoma.
Cancer Immunol Res; 6(10); 1234–45. ©2018 AACR.

Introduction

Non–small cell lung cancer (NSCLC), comprising lung adenocarcinoma, squamous-cell lung carcinoma, and large cell carcinoma, makes up 85% to 90% of lung cancers, and the different subtypes differ in genomic features and clinical histories (1). Mutation of *KRAS*, encoding a small GTPase linking growth factor signaling and downstream MAPK signaling, is present in approximately 30% of lung adenocarcinoma and associates with poor prognosis in NSCLC (2, 3). Although drugs such as MEK inhibitors and PI3K inhibitors are under investigation in NSCLC, there is no approved therapy directly targeting this oncogene (2, 3). Furthermore, *KRAS* mutation concurrent with other genetic alterations provokes differential responses to current therapeutics and therapeutic resistance (4, 5). For example, *TP53* or *LKB1* comutation makes *KRAS*-mutant tumors more resistant to chemotherapy (4). These concurrent genetic lesions are also associated with lung tumors that are characterized by distinct immune cells dynamics within the tumor microenvironment (5). In a preclinical study of $Kras^{+/LSL\text{-}G12D}$; $Trp53^{L/L}$ (KP) genetically engineered mice (GEM), the concurrent p53 deficiency rendered KP tumors more chemoresistant, compared with either *Kras* alone or *Kras* with concurrent *Lkb1* mutation (4). Considering the high rate of p53 deficiency in *KRAS*-mutant NSCLCs, an urgent need exists to explore new therapeutic modalities targeting this NSCLC subset.

[1]Laura & Isaac Perlmutter Cancer Center, New York University Langone Medical Center, New York, New York. [2]Department of Medical Oncology, Dana-Farber Cancer Institute, Harvard Medical School, Boston, Massachusetts. [3]Broad Institute of Harvard and MIT, Cambridge, Massachusetts. [4]Oncology Innovative Medicines Unit, AstraZeneca R&D Boston, Waltham, Massachusetts. [5]Department of Pathology, Shanghai Tongji Hospital, Tongji University School of Medicine, Shanghai, China. [6]Applied Bioinformatics Laboratories and Department of Pathology, New York University School of Medicine, New York, New York. [7]Belfer Institute for Applied Cancer Science, Dana-Farber Cancer Institute, Boston, Massachusetts. [8]Novartis Institutes for Biomedical Research, Cambridge, Massachusetts. [9]Department of Biochemistry and Molecular Biology, Hollings Cancer Center, Medical University of South Carolina, Charleston, South Carolina. [10]Division of Gastroenterology, Departments of Medicine and Genetics, Abramson Cancer Center, University of Pennsylvania Perelman School of Medicine, Philadelphia, Pennsylvania.

Note: Supplementary data for this article are available at Cancer Immunology Research Online (http://cancerimmunolres.aacrjournals.org/).

D.O. Adeegbe and S. Liu contributed equally to this article.

Corresponding Authors: Kwok-Kin Wong, New York University Langone Medical Center, 550 1st Avenue, New York, NY 10016. Phone: 212-263-9203; Fax: 212-263-9210; E-mail: Kwok-Kin.Wong@nyumc.org; and Dennis O. Adeegbe, Dennis.Adeegbe@nyumc.org

doi: 10.1158/2326-6066.CIR-18-0077

Published OnlineFirst August 7, 2018; DOI: 10.1158/2326-6066.CIR-18-0077

Epigenetic mechanisms such as acetylation, methylation, and phosphorylation regulate gene transcription without altering the genetic code (6, 7). Proteins with epigenetic functions can be categorized into three main types: writers (such as DNA methyl transferases; DNMT), readers (such as bromodomain proteins), and erasers (such as histone deacetylases; HDAC; refs. 8–10). As a consequence of their activities, these epigenetic enzymes modulate many biological processes, and their hyperactivity or overexpression has been reported in a number of cancers (8). Accumulating evidence demonstrates that a number of pharmacologic agents targeting these proteins elicit cytostatic and/or cytotoxic effects in tumor cells (9). Given reported contributions of immune cells to durable antitumor responses (11, 12), caution should be exercised in utilization of these agents for oncologic therapeutic applications as deleterious effects on tumor-associated immune cells may impede immune-orchestrated antitumor responses. In this vein, JQ1, an inhibitor of the BET family of bromodomain-containing proteins, may be a promising epigenetics-targeting drug for the treatment of NSCLC due to its reported efficacy in hematologic malignancies such as acute myeloid leukemia and multiple myeloma, as well as in other investigational solid cancer models (13–16). Our previous study demonstrated antitumor activity of JQ1 in *KRAS*-mutant lung cancers, either as a single agent or in combination with HDAC inhibitors (17, 18). However, the therapeutic efficacy of this combination in these settings is still somewhat limited.

Immunotherapy, in particular, the rapid development of multiple immune checkpoint blockade molecules, is among the most exciting recent breakthroughs in cancer treatment (12, 19). Immune therapies such as PD-1/PD-L1 and CTLA-4–blocking antibodies have been approved in multiple advanced and metastatic cancers, including NSCLC (11, 20). Immunotherapy promotes greater duration of survival in some patients than conventional chemotherapies in some lung cancer subtypes (21, 22). However, with the exception of melanoma, the majority of patients with cancer do not exhibit clinical benefit from anti–PD-1 therapy due to a variety of resistance mechanisms stemming from the lack of presentation of effective antigens, JAK1/2 mutations, and other immune response alterations (23–25). Thus, a critical unmet need remains to develop combination therapies to expand the group of immunotherapy responders. This notion is supported by our previous studies in which anti–PD-1 showed efficacy in certain subtypes of *Egfr*-mutant lung cancer GEM (26), and when coupled with radiotherapy in *Kras*-mutant tumors (27).

Immunosuppressive mechanisms, such as PD-1 expression on tumor-infiltrating T cells, and accumulation of suppressive T cells, such as $CD4^+Foxp3^+$ regulatory T cells (Treg), in the tumor microenvironment impede antitumor immune responses. Several lines of evidence demonstrate that eliminating such inhibitory mechanisms in tumors can pave the way for a more productive antitumor response, thereby facilitating a tumor microenvironment where immune stimulatory signals prevail over inhibitory ones. In the present study, we hypothesized that combining JQ1, which we previously demonstrated disrupts tumor-Treg function (18), with anti–PD-1 blockade will alleviate potential tumor-reactive effector T cells of the inhibitory barriers posed by PD-1 signaling and Treg presence to favor enhanced T-cell function within the tumor milieu. We tested this hypothesis by evaluating the effects of both agents on phenotypic and functional features of tumor-infiltrating T cells, upon their administration in a genetically engineered mouse model (GEMM) of NSCLC in which lung tumor development is driven by activating Kras mutation and p53 deficiency (KP). Furthermore, the therapeutic potential of this unique combinatorial regimen in this NSCLC model was explored.

Materials and Methods

Mice

All breeding and treatment experiments were performed with the approval of DFCI Animal Care and Use Committee. Mice were maintained under specific pathogen-free conditions in an AAALAC-accredited facility. All animal work was conducted in accordance with ARRIVE guidelines (28).

Kras$^{+/LSL\text{-}G12D}$; *Trp53*$^{L/L}$ (KP) GEMs and treatment studies

KP mice were induced with adeno-Cre intranasally, and lung tumors were confirmed and monitored by magnetic resonance imaging (MRI) with BioSpec USR70/30 horizontal bore system (Bruker; ref. 4). 3D Slicer software was used to quantify the tumor volume (4). After MRI confirmation of tumors, KP mice were treated with JQ1 (50 mg/kg i.p. daily), anti–PD-1 (clone 29F.1A12; 200 μg/mouse i.p. 3 times per week), or in combination, and tumor growth was monitored by MRI every 2 weeks. For depleting antibody treatments, anti-CD4 (GK1.5) and anti-CD8 (53-6.72) were purchased from Bio X Cell. Mice in each group were given 2 consecutive doses (400 μg/mouse) of antibodies at day −2 and day −1 and twice per week thereafter together with JQ1/α-PD-1 combination treatment.

Adoptive T-cell transfer and tumor inoculation studies

For adoptive transfer and tumor inoculation studies in athymic nude mice, transthoracic injection of KP cell line (2×10^6) was first performed. Upon establishment of lung tumors as confirmed by MRI, total $CD4^+$ or $CD4^+CD25^-$ T cells (2.5×10^6) isolated from KP mice were transferred i.v. into these tumor-bearing mice. Two weeks later, the phenotype of the transferred $CD4^+$ T cells present in tumors were analyzed. KP cell lines were established in our laboratory using lung tumor nodules of genetically engineered *Kras*$^{+/LSL\text{-}G12D}$;*Trp53*$^{L/L}$ (KP) mice. All cell lines were authenticated by DNA fingerprinting and verified as *Mycoplasma*-free using Universal Mycoplasma Detection Kit (ATCC).

Immune profiling with multicolor flow cytometry

Tumor-bearing mouse lungs were collected from KP mice after which tumor nodules were excised and cut into about 1 mm pieces before placement under Hank's Balanced Salt Solution containing 100 U/mL Collagenase D from *Clostridium histolyticum* (Sigma-Aldrich) and 50 μg/mL DNase I grade II from bovine pancreas (Sigma-Aldrich) for 40 minutes at 37°C. After digestion, cells were passed through a 70-μm strainer to remove clumps and treated with ACK Lysing Buffer (Life Technologies). Cells were resuspended in FACS buffer (PBS + 2% fetal bovine serum) for flow cytometry. For multicolor flow cytometry, cells were first stained with LIVE/DEAD Fixable Aqua Dead Cell Stain Kit, for 405 nm excitation (Life Technologies) for 30 minutes at 4°C and washed twice with FACS buffer. Cells were treated with purified anti-mouse CD16/32 (BioLegend) for 15 minutes, and then antibody mixture was added. Thirty minutes later, the cells were washed twice with FACS buffer and fixed in 1% formalin or further processed for intracellular staining. For intracellular staining, cells were fixed/permeabilized with Foxp3/Transcription

Published OnlineFirst August 7, 2018; DOI: 10.1158/2326-6066.CIR-18-0077

Factor Staining Buffer Set Kit (eBioscience) before antibodies were added. After two washes, samples were resuspended in FACS buffer before acquisition using BD LSRFortessa or BD FACSCanto (BD Biosciences).

Antibodies

All antibodies used for flow cytometry analysis were purchased from BD Biosciences, BioLegend, or eBioscience and are listed in Supplementary Table S1.

Ex vivo CD8$^+$ T-cell activation assay

Leukocytes from lungs of treated mice were isolated using Ficoll gradient separation after single cell disassociation. Then, 10^6 isolated cells were stimulated at 37°C with Leukocyte Activation Cocktail for 6 hours with FITC-CD107a (BioLegend) and BD GolgiPlug (BD Pharmingen) added in the last 5 hours. Cells were washed and stained for intracellular cytokines using BD cytofix/cytoperm kit (BD Pharmingen) according to the manufacturer's instructions.

Ex vivo tumor cell death assay

EpCAM$^+$ tumor cells and CD3$^+$Foxp3$^-$ T cells were sorted from the tumors of treated mice. Cells were rested in complete media for 1 hour, after which 1×10^5 T cells were added to 1×10^3 tumor cells in 96-well plate and incubated at 37°C for 24 hours in the presence of 5 IU/mL of IL2. Tumor cell death was assessed by FACS staining using fixable live/dead dye.

T-cell proliferation/Treg-suppression assay

For mouse Treg-suppression assays, CD4$^+$CD25^{hi} Tregs in tumor cell suspensions were sorted into KLRG1$^+$ or KLRG1$^-$ cells and cultured at 1:2, 1:4, and 1:8 ratios with carboxyfluorescein diacetate succinimidyl ester (CFSE)–labeled CD4+CD25$^-$ cells (0.25×10^5) isolated from the spleen of the same mouse. T-cell–depleted, mitomycin C–treated splenocytes (0.25×10^5) were added as antigen-presenting cells, and cultures were stimulated with soluble anti-CD3 (clone 2C11; eBioscience) at 0.5 μg/mL concentration for 3 days.

Cytokine analysis

Bronchoalveolar lavage (BAL) fluid was collected from the tumor-bearing lungs of KP mice by injecting 0.5 mL of 1× PBS into the lungs with repeated flushing before dispensing into collection tubes. BAL fluids were then immediately centrifuged for 5 minutes at 1,200 rpm at 4°C and subsequently stored at −80°C and thawed on ice prior to analysis. Each assay used 50 μL of each sample. A multiplex magnetic bead-based sandwich ELISA assay was utilized to simultaneously measure 23 secreted proteins, including IL4, RANTES, KC, G-CSF, IL17, IL5, IL1α, IL9, MIP-1β, MIP-1α, MCP-1, IL13, IL12 (p70), IL12 (p40), IL3, Eotaxin, GM-CSF, IFNγ, IL10, IL1β, IL2, IL6, and TNFα, which were tested in a single assay format (Bio-Rad: Bioplex 23× ms panel; cat. #M60009RDPD). Each bead is encoded with a ratiometric concentration of 2 IR dyes and acts as a barcode, unique to each protein. The final detection complex is formed with the addition of streptavidin–phycoerythrin conjugate, where the phycoerythrin serves as the fluorescent reporter. Concentration levels, measured in pg/mL, for each cytokine are derived from 5-parameter curve fitting models. Fold changes relative to control are calculated and plotted as log2FC to establish biological significance.

RNA-seq and data analysis

A small portion of snap-frozen lung tumor from each mouse was pulverized using the Covaris T-prep method on dry ice (cat. #520097). The Agencourt RNAadvance kit for isolation of nucleic acids from frozen tissue (cat. #A32645) was implemented on a Biomek FXP Laboratory Automation Workstation (dual arm system with multichannel pipette and span-8 pipetters; cat. #A31844). The automated protocol is based upon Solid Phase Reversible Immobilization paramagnetic bead-based technology, which does not require vacuum filtration, centrifugation, or organic solvents such as phenol or xylene associated with traditional methods. Briefly, the tissue is lysed, after which the RNA is immobilized onto the magnetic particles. The RNA is then treated with DNase and the contaminants rinsed away using a simple wash procedure. RNA isolates were eluted in a 55 μL volume of RNase/DNase-free H_2O. All RNA was stored at −80°C. RNA quality was assessed by Agilent Bioanalyzer using the RNA 6000 pico kit (cat. #5067-1513). Fifty nanograms RNA was utilized as input for RNA-seq library preparation utilizing the TruSeq RNA Access Library Prep Kit (cat. #RS-301-2001). The method was automated on the Biomek FXP Laboratory Automation Workstation. This method facilitates enrichment of the coding regions of the transcriptome that are captured using sequence-specific probes to create the final library. cDNA libraries were quantified utilizing the Quanti-iT PicoGreen assay (Life Technologies, cat. #P7589). One microliter of cDNA was required for quantification. Concentration is measured as ng/μL. Libraries were excited at 480 nm, and the fluorescence emission intensity was measured at 520 nm using a Victor X3 spectrophotometer (PerkinElmer; cat. #2030-0030). Fluorescence intensity was plotted versus concentration over the low calibration range, 0–50 ng/μL. Libraries were also quality checked by Agilent Bioanalyzer using the High Sensitivity DNA Kit (cat. #5067-4626). cDNA libraries were then sequenced on the Illumina NextSeq500 platform as 75-bp paired end reads. The STAR RNA-seq alignment tool (Spliced Transcripts Alignment to a Reference) aligner [STAR_2.5.0a]) was utilized to align the data to the mouse genome (RefSeq gene annotations). DeSeq2 (29) was utilized to perform differential expression analysis. We conducted pathway enrichment analysis utilizing the GeneGo MetaCore + MetaDrug tool (Thompson Reuters, version 6.31 build 68930). RNA-seq data have been deposited in the NCBI GEO public data repository (reference series accession GSE114601).

Mouse-derived organotypic tumor culture

Mouse-derived organotypic tumor cultures were established from gently dissociated KP tumors, after which the generated tumor spheroids were mixed with supporting collagen matrix and loaded into three-dimensional AIM glass chambers (AIM Biotech) in the presence of complete media containing JQ1 (250 nm) and anti–PD-1 (10 μg/mL). DMSO served as a control. After 3 days in culture, media were aspirated and chambers were gently washed with 1× PBS prior to immunofluorescent staining. Briefly, purified CD16/32 FCγR-blocking reagent was added to chambers for 15 minutes at room temperature followed by Alexa Fluor 488 anti-mouse CD3 and Alexa Fluor 594 anti-mouse EpCAM for 1 hour. Then, chambers were washed gently with 1× PBS/2% FBS twice and DAPI (Invitrogen; 1:1,000×) was added and incubated for 5 minutes followed by two washes with 1× PBS/2% FBS. Images were captured on a Nikon Eclipse 80i fluorescence microscope equipped with CoolSNAP CCD camera and merged images

Published OnlineFirst August 7, 2018; DOI: 10.1158/2326-6066.CIR-18-0077

created with NIS elements imaging software. Quantification of $CD3^+$ T cells under each treatment condition was determined from an average of 10 to 11 fields of view as evaluated by fluorescent microscopy.

Statistical analysis

Data were analyzed using mean ± standard error of the mean (SEM). An unpaired two-tailed Student *t* test was used for comparisons between two groups using GraphPad Prism software. *P* values < 0.05 were considered statistically significant (*); *P* values < 0.01 are marked **, and *P* values < 0.001 are marked ***.

Results

PD-1 blockade and BET bromodomain inhibition attenuates PD-1 expression and Treg proportions

In previous studies, we demonstrated that JQ1, an inhibitor of BET family of bromodomain (BRD) proteins, disrupts Treg phenotype and function in tumors of GEMM of NSCLC (18). Existing reports also show that, although clinical responses seen in patients treated with PD-1 blockade can be remarkable, these therapeutic benefits are limited to a subset of patients (20, 23, 24). Consistent with this, only two of the six GEM-harboring *Kras*-driven lung adenocarcinomas showed a delay in tumor growth following PD-1 treatment (ref. 27; Supplementary Fig. S1). We hypothesized that combining JQ1 with PD-1 blockade would dampen the cellular and molecular inhibitory mechanisms ascribed to Treg function and PD-1 signaling, respectively, to favor improved T-cell activation and function within the tumor-immune microenvironment. To test this hypothesis, we used the use of GEM-harboring activating *Kras* mutations with concurrent *p53* deficiency (KP; Fig. 1A), with the rationale that this model mirrors clinical presentations of aggressive lung adenocarcinomas driven by *KRAS* mutations and/or *p53* deficiency. First, we evaluated KP mice treated with JQ1/anti–PD-1 for 2 weeks in order to characterize changes to immunologic parameters accompanying these treatments (Fig. 1A). Although the numbers of cells in most of the tumor $CD45^+$ leukocyte subpopulations that we evaluated did not significantly change (Supplementary Table. S2; Supplementary Fig. S2), the proportion of $CD4^+Foxp3^+$ Tregs decreased about 60% in JQ1 and JQ1/anti–PD-1-treated mice, relative to vehicle controls (Fig. 1B). Comprehensive profiling of tumor-infiltrating $CD4^+$ and $CD8^+$ T cells revealed that among several immune checkpoint receptors evaluated, the frequency of PD-1–expressing T cells, which is more prominently expressed than CTLA-4 on tumor-infiltrating T cells (Supplementary Fig. S3), was diminished after JQ1 treatment with or without anti–PD-1 but not with anti–PD-1 treatment alone ($CD8^+$ T cells in Fig. 1C; $CD4^+$ T cells in Supplementary Fig. S4A). A modest decrease in T-cell expression of CTLA-4 was also observed upon PD-1 treatment, which was significant when combined with JQ1 administration (Fig. 1D; Supplementary Fig. S4B). These changes were not observed in peripheral (splenic) T cells where PD-1 and CTLA-4 were only expressed at basal levels (Supplementary Fig. S3). Taken together, these results demonstrate quantitative and phenotypic changes on Tregs and potential effector T cells, respectively, that is consistent with reduced cellular and molecular inhibitory entities in tumor-infiltrating T cells upon combined administration of JQ1 and anti–PD-1 in NSCLC-bearing mice.

PD-1 blockade combined with BET bromodomain inhibition enhances T-cell activation and effector activity

Given that T-cell activation and function is most permissive under reduced expression of molecular inhibitors and/or hindrance by suppressive cells, we tested whether our findings above correlate with effector activity by evaluating the activation status and functional capacity of tumor-infiltrating T cells in the treated GEM. Phenotypic assessments showed that tumor-infiltrating $CD4^+$ and $CD8^+$ T cells exhibited an increased activation profile under anti–PD-1 or JQ1 treatment, given by increased frequencies of $CD69^+$ T cells, an effect that was further amplified upon their combination (Fig. 2A and B). Upon *ex vivo* stimulation, tumor-infiltrating $CD8^+$ T cells under single-agent treatment exhibited an augmented ability to secrete the effector cytokine IFNγ and the expression of degranulation-associated membrane protein CD107a. This increased effector profile was most pronounced upon combination of JQ1 and anti–PD-1 (Fig. 2C and D), indicating that both agents cooperatively promote enhanced activation and effector function of $CD8^+$ T cells in the tumor bed. Similar findings for IFNγ were also noted for tumor-$CD4^+$ T cells (Supplementary Fig. S4C). This reinvigoration in T-cell effector function likely stems in part from the diminished PD-1 expression on tumor-T cells, as their capacity to secrete the effector cytokine IFNγ inversely correlated with frequency of PD-1^+ T cells (Supplementary Fig. S4D). Although analysis of myeloid cells ($CD45^+CD11b^+$/$CD45^+CD11c^+$) did not reveal broad phenotypic changes, treatment with JQ1 alone or with anti–PD-1 was accompanied by increased expression of MHC class I on tumor-associated macrophages (TAM), which also exhibited modest decrease in PD-L1 expression (Supplementary Fig. S5A–S5C). Of note, JQ1 treatment also evoked measurable effects on tumor cells, such as downregulation of genes encoding tumor growth and survival proteins, as well as concurrent upregulation of a number of tumor suppressors (Supplementary Fig. S6; Supplementary Table. S3).

Combination of anti–PD-1 and JQ1 evokes a Th1 cytokine signature in the local tumor niche

The cytokine milieu within or around tumor microenvironment plays crucial roles in regulating cell-mediated immunity (30–32). We therefore asked how the cytokine composition associated with the tumor niche is affected by anti–PD-1 and JQ1 treatment. We analyzed the BAL fluid within the local tumor-bearing lung of treated KP mice. Relative to the vehicle treatments, a number of cytokines that regulate T lymphocyte differentiation or signify their functional tendencies, including IL2, IL12, IFNγ, and TNFα, were increased in the BAL fluid of JQ1 or anti–PD-1-treated mice whereas IL4, IL5, IL6, IL10, and IL13 were either decreased or marginally increased. These patterns appeared somewhat additive under combined JQ1/anti–PD-1 treatments, resulting in greater changes than associated with either agent alone (Fig. 3A). Dissecting the pattern of the T-cell–related cytokines further, we found that as compared with vehicle control treatment, a Th1 cytokine profile, including elevated IL12 (p40), TNFα, and IFNγ, was more dominant in the BAL fluid associated with tumors of single-agent–treated KP mice when assessed against Th2 cytokines IL4, IL5, IL10, and IL13. As with previous phenotypic changes, this bias in favor of Th1 cytokines was most striking with the combination of JQ1 and PD-1 (Fig. 3B and C), demonstrating that an overall effector cytokine profile is evoked under the combinatorial regimen. A number of cytokines

Published OnlineFirst August 7, 2018; DOI: 10.1158/2326-6066.CIR-18-0077

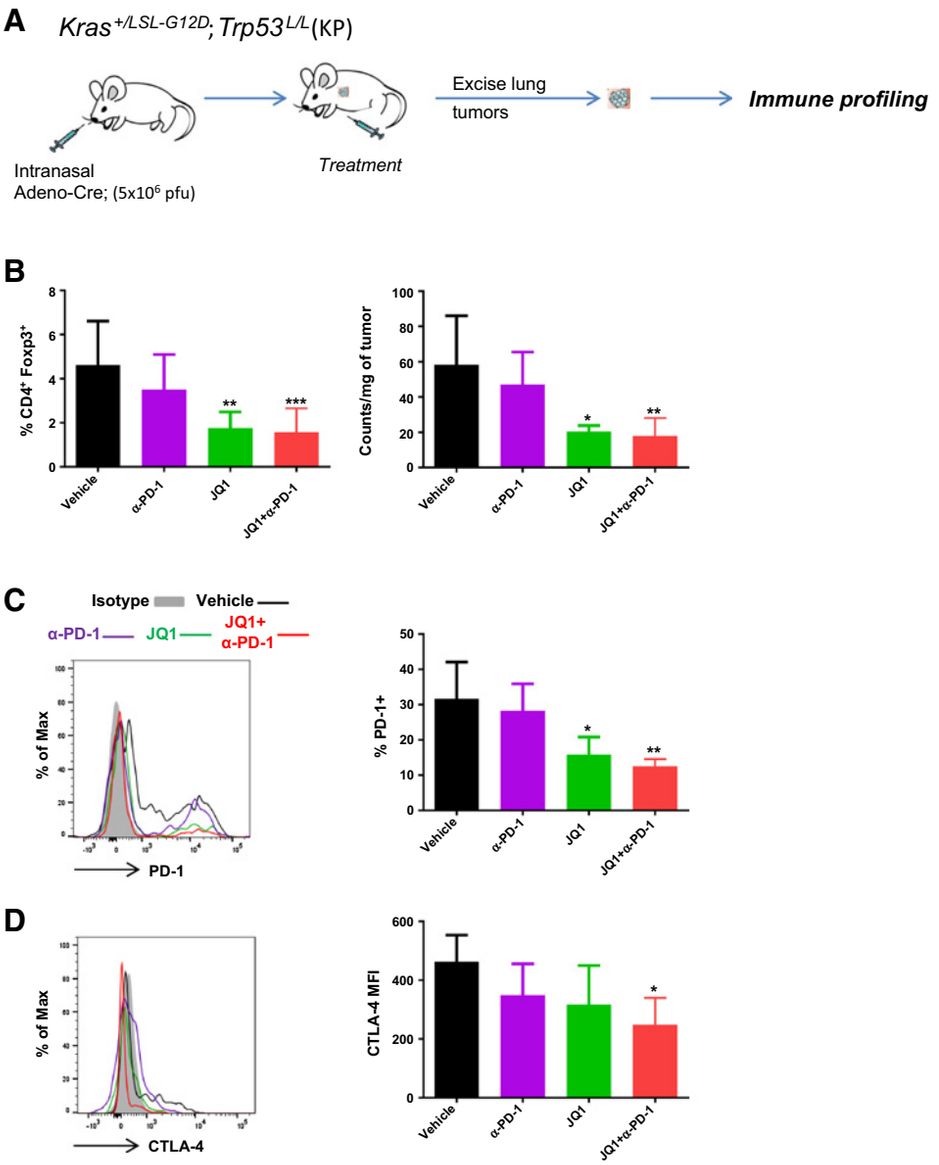

Figure 1.

PD-1 blockade and BET bromodomain inhibition promotes reduced Treg proportions and expression of inhibitory receptors on tumor-infiltrating T cells in GEMM of NSCLC. **A,** Schematics of treatment study and immune analysis in KP GEM. KP mice were induced with adeno-Cre intranasally, and treatment was started upon tumor establishment as confirmed by MRI. After 2 weeks of treatment, tumor nodules were excised from the lungs of JQ1 and/or α-PD-1–treated mice, and multiparameter flow-cytometric analysis was conducted on single cell suspensions to assess the frequencies and phenotype of tumor-infiltrating T-cell subsets. **B,** Percent $CD4^+Foxp3^+$ Tregs within $CD45^+$ leukocytes (left) and absolute Treg counts within the tumors of KP mice treated as indicated. **C** and **D,** Representative histograms (left) and summary (right) of expression levels for (**C**) PD-1 and (**D**) CTLA-4 on tumor-infiltrating $CD8^+$ T cells. Data are mean ± SEM for 4–5 mice per group. *, $P < 0.05$; **, $P < 0.01$; ***, $P < 0.001$.

implicated in myeloid cell trafficking and recruitment (e.g., MCP-1, MIP-1, RANTES, and Eotaxin) were also substantially elevated in the combination treatment (Fig. 3A).

Combination of JQ1 and anti–PD-1 delays tumor growth and improves survival of KP mice

Based on the enhanced effector profile of tumor-infiltrating T cells following JQ1 and anti–PD-1 treatment, we hypothesized that the combination of both agents should potentiate an improved antitumor response in long-term treatment studies. Thus, to evaluate the therapeutic potential of this drug combination, KP mice were assessed by MRI every 2 weeks during the course of single- and dual-agent treatment, and tumor volume was quantified. Although anti–PD-1 treatment led to moderate delay in tumor progression (change in tumor volume of ~10%–30%) relative to vehicle treatment, JQ1 administration resulted in a more robust tumor growth arrest and shrinkage (change in tumor volume of −10%–10%) at 2 weeks after treatment initiation. Tumors regressed in all mice with combination therapy (Fig. 4A and B). Although PD-1 alone promoted a modest improved overall survival of tumor-bearing mice relative to control treatment [median survival time (MST) 36 days vs. 16 days], JQ1 treatment resulted in a significantly prolonged survival that was further increased under the combination therapy (Fig. 4C; MST 69 and 87, respectively). In separate cohorts, we found that the addition of CD8- or CD4-depleting antibodies to the JQ1/anti–PD-1 combination regimen led to substantial or modest loss of antitumor response and survival benefits, respectively, suggesting that the protection from tumor progression under this drug combination is largely immune (T-cell) mediated (Fig. 4A and C). In support of this notion, treatment of immunodeficient mice bearing similar lung tumors as the GEM showed only marginal or slightly modest improvement in their overall survival when treated with anti–PD-1 or JQ1, respectively

Published OnlineFirst August 7, 2018; DOI: 10.1158/2326-6066.CIR-18-0077

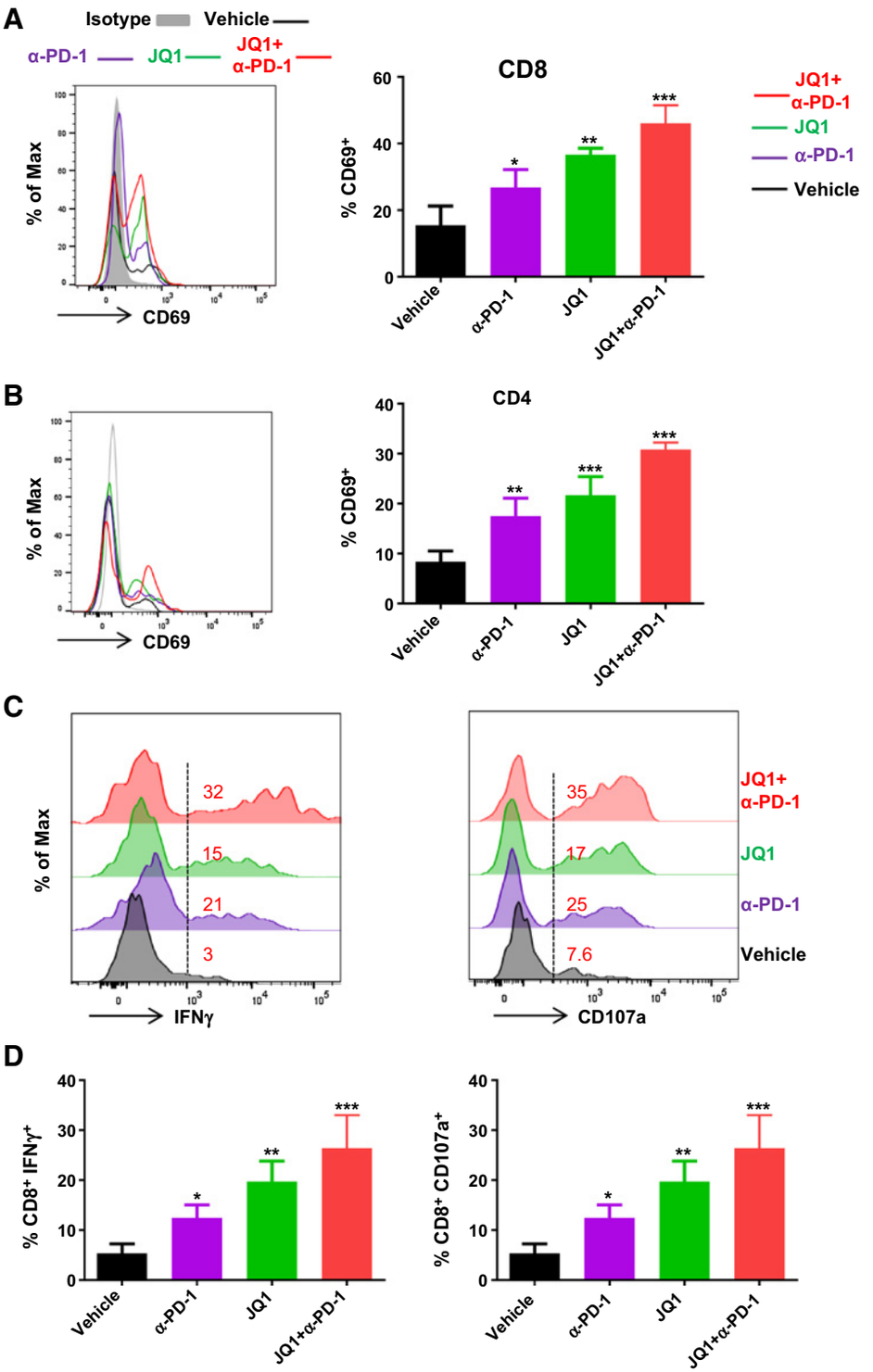

Figure 2.

PD-1 blockade and BET bromodomain inhibition promote increased activation and effector capacity of tumor-infiltrating T cells in GEMM of NSCLC. Phenotypic assessments were conducted by flow cytometry of tumor cell suspensions to evaluate activation status of T cells. **A** and **B,** Representative histograms (left) and summary (right) of CD69 expression on tumor-infiltrating (**A**) $CD8^+$ and (**B**) $CD4^+$ T cells. **C** and **D,** Immune cells from KP tumors treated with vehicle or indicated agents were isolated by Ficoll gradient and stimulated for 6 hours with leukocyte activation cocktail (PMA and ionomycin); GolgiPlug and CD107a antibody were added in the last 5 hours of culture. **C,** Representative histograms with corresponding percentages and (**D**) summary of $CD8^+$ T cells secreting IFNγ after intracellular cytokine staining. Data are mean ± SEM for 3–4 independent experiments. *, $P < 0.05$; **, $P < 0.01$; ***, $P < 0.001$.

(Supplementary Fig. S7). Furthermore, and consistent with the *in vivo* therapeutic outcomes, $CD8^+$ T cells that were isolated from tumors of treated KP mice showed enhanced degranulation and cytotoxic activity *in vitro* that paralleled increased tumor cell death. This effect was most robust with JQ1/anti–PD-1 combination therapy, providing evidence linking the augmented activation/effector profile evoked in this treatment setting with antitumor activity (Supplementary Fig. S8A–S8C). Underscoring the relatively safe profiles of this JQ1/anti–PD-1 combination was the lack of deleterious effect on the overall proportions of tumor-associated T cells (Supplementary Fig. S9). Collectively, these data demonstrate that partnering immune checkpoint blockade with

Published OnlineFirst August 7, 2018; DOI: 10.1158/2326-6066.CIR-18-0077

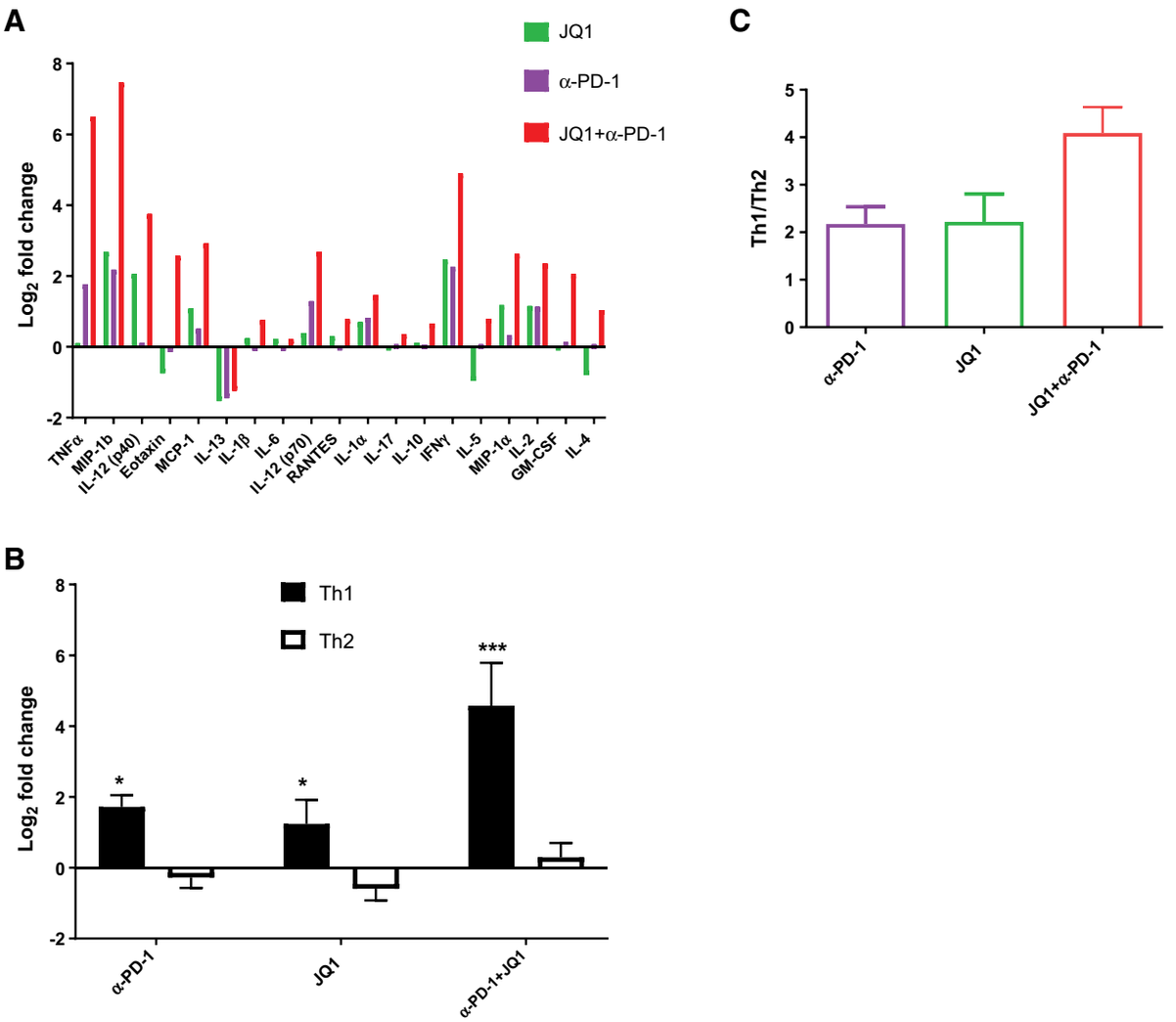

Figure 3.

PD-1 blockade and BET bromodomain inhibition is associated with a Th1 cytokine skewing in the BAL fluid of treated GEMM of NSCLC. BAL fluid obtained from the lungs of KP-tumor–bearing mice treated with α-PD-1, JQ1, or the combination was subjected to multiplex cytokine evaluation. **A,** Summary of listed cytokines detected in the BAL fluid of mice that were treated as indicated shown as $\log_2$ fold change relative to samples from vehicle-treated mice. **B,** Mean fold change for Th1 (IL2, IFNγ, and TNFα) and Th2 (IL4, IL5, IL6, IL10, and IL13) cytokines relative to the vehicle controls in BAL fluids. **C,** Ratio of the mean values for Th1 versus Th2 cytokines concentrations. Data in **A** are the average value for 4 replicates expressed as $\log_2$ fold change over vehicle for each cytokine. Data shown in **B** and **C** represent mean ± SEM for 4 replicates/group. *, $P < 0.05$; ***, $P < 0.001$.

BET bromodomain inhibition improved antitumor T-cell function and led to robust and long-lasting therapeutic outcomes in the aggressive *Kras/p53*-mutant NSCLC.

Diminished KLRG1$^+$ Tregs associate with increased survival following JQ1/anti–PD-1 treatment

Unlike in the spleen, a prominent proportion of CD4$^+$Foxp3$^+$ Tregs infiltrating the tumors of KP mice express KLRG1 (Fig. 5A), a cell surface protein that has been linked to terminally differentiated T cells (33). Although there is generally an accumulation of tumor-infiltrating Tregs with increasing tumor burden, we found that the KLRG1$^+$ Treg subset (Fig. 5B) showed a direct correlation with tumor size. We hypothesized that this KLRG1-expressing, tumor-infiltrating Treg subset represents a distinct Treg fraction, the characterization of which could provide clues to their molecular features and functional activities. To test this hypothesis, further phenotypic and functional studies were conducted. Analysis of these KLRG1$^+$ Treg subset revealed that they are more activated, as indicated by the vast majority being CD69$^+$, CD44^{hi}, and CD62L^{lo}, when compared with their KLRG1$^-$ counterparts or peripheral pool of splenic Tregs (Supplementary Fig. S10A). Despite this distinction, their high expression of Helios and Neuropilin-1, two proteins that are highly expressed on natural Tregs, mirrored that of the KLRG1$^-$ cells and splenic Tregs, suggesting that the KLRG1$^+$ Tregs likely arise from the peripheral pool of naturally occurring Tregs of thymic origin (Supplementary Fig. S10B). We next used an orthotopic tumor model by injecting KP tumor cells transthoracically and subsequently performed

Published OnlineFirst August 7, 2018; DOI: 10.1158/2326-6066.CIR-18-0077

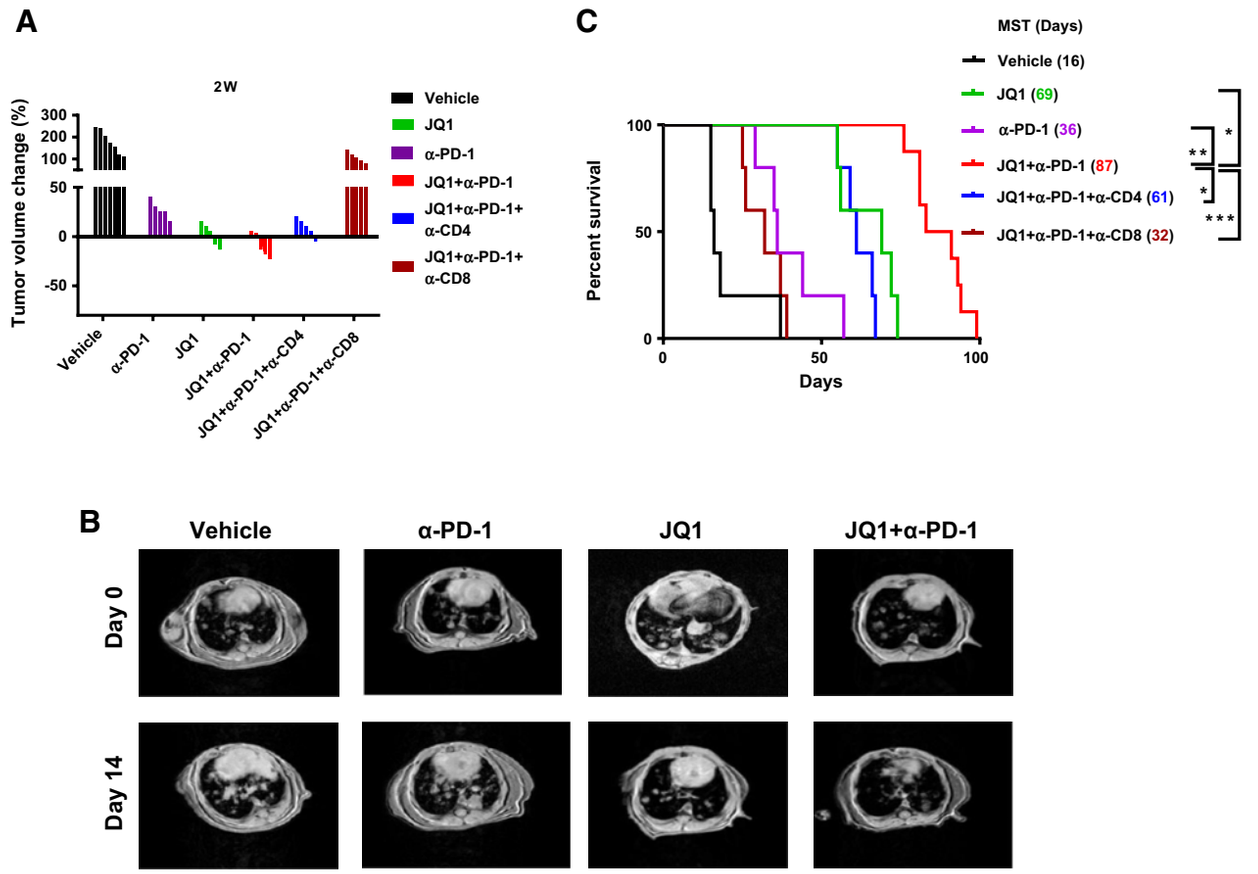

Figure 4.

Combination of BET bromodomain inhibitor and anti–PD-1 promotes long-lasting therapeutic outcomes in KP-driven lung adenocarcinomas. **A,** Waterfall plots showing tumor volume change (%) under indicated treatments after 2 weeks compared with pretreatment tumor burden. Each column represents one individual mouse under each treatment. **B**, Representative MRI images of lung tumors in KP mice on day 0 and day 14 after vehicle (control), JQ1, and/or α-PD-1 treatments. **C,** Overall survival curve of KP mice under each indicated treatment with corresponding median survival time in days. Data are from 5–7 mice/treatment group. *, $P < 0.05$; **, $P < 0.01$; ***, $P < 0.001$.

adoptive transfer of $CD4^+$ T cells, which were isolated from spleens of KP mice (Supplementary Fig. S11A). Analyses of the input cells, which were either bulk $CD4^+$ T cells or a subset depleted of $CD25^+$, showed that the major $Foxp3^+$ population within the $CD25^+$ subset or the minute $Foxp3^+$ fraction within the $CD25^-$ subset did not express KLRG1 at time of transfer (Supplementary Fig. S11B). Two weeks after transfer of either the bulk $CD4^+$ T cells or $CD25^-CD4^+$ population, the lung tumors were collected and the T cells were analyzed. A sizable pool of tumor-infiltrating $KLRG1^+$ $CD25^+Foxp3^+$ Tregs was readily detected in the lung tumors of mice that received $CD4^+$ T cells containing a largely $KLRG1^-$ Treg pool. In contrast, $CD4^+CD25^-$ conventional T cells that were transferred into parallel cohorts of tumor-bearing mice largely retained their $Foxp3^-$ phenotype. The few $Foxp3^+$ cells that were present in the tumors were $CD25^{dim/-}$ and did not generate a detectable KLRG1-expressing subpopulation (Supplementary Fig. S11C). These data demonstrate that the $KLRG1^+$ Treg pool is a derivative of $CD25^+Foxp3^+$ Tregs and not a peripherally induced subset converted from $CD25^-$ conventional $CD4^+$ T cells.

As CTLA-4 is critical for Treg function, we also found that the tumor-associated $KLRG1^+$ Tregs exhibit higher CTLA-4 levels that parallels their superior suppressive function compared with their $KLRG1^-$ counterparts (Supplementary Fig. S12A and S12B). Given our observations *in vivo*, we then examined whether there is any correlation between the presence of these cells and the therapeutic responses observed. Whereas a moderate decrease in proportion of $KLRG1^+$ Tregs was observed in the tumors of anti–PD-1-treated mice, a significant reduction was observed following JQ1 monotherapy and was further reduced by 5% to 10% following treatment in combination with anti–PD-1 (Fig. 5C and D). Consistent with their decline under JQ1 treatment (Fig. 5D), the $KLRG1^+$ Treg fraction exhibited diminished expression of Foxp3, CTLA-4, GITR, and Bcl-2 compared with the negative subset, suggesting that JQ1 evokes a greater disruption to their molecular features, compared with anti–PD-1, along with a propensity toward reduced survival (Supplementary Fig. S13). Lastly, the inverse relationship between the $KLRG1^+$ Treg frequency and overall survival in the treatment settings (Fig. 5E) suggests that terminally differentiated KLRG1-expressing Treg proportions in the tumor may be a surrogate for severity of disease and their reduction associated with therapeutic response.

Published OnlineFirst August 7, 2018; DOI: 10.1158/2326-6066.CIR-18-0077

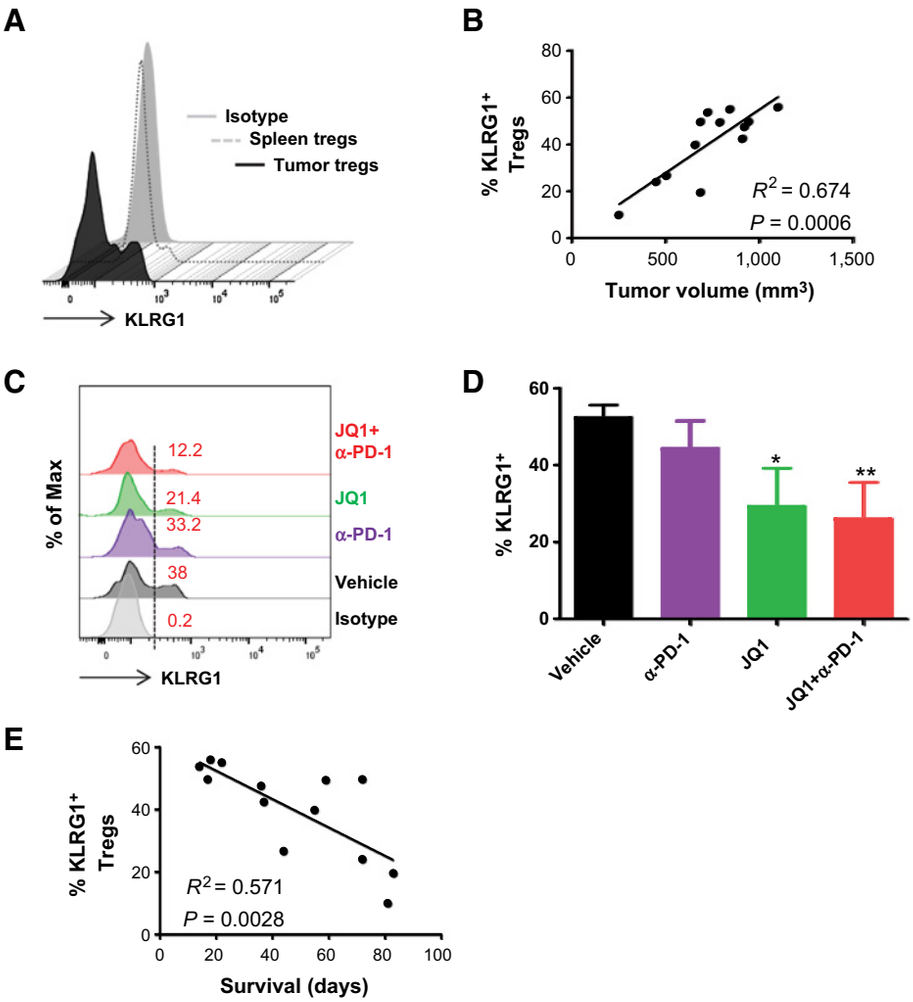

Figure 5.

Reduced proportions of KLRG1$^+$ Tregs are associated with low tumor burden and improved survival and response to treatment in KP mice. Following identification of a subset of tumor-infiltrating KLRG1$^+$ CD4$^+$Foxp3$^+$ Tregs, their proportions were further assessed. **A,** Representative histograms for the expression of KLRG1 on splenic versus tumor Tregs. **B,** Percentage of KLRG1$^+$ Tregs in the tumors of KP mice as a function of tumor volume. **C,** Representative histograms with corresponding percentages and (**D**) summary of KLRG1$^+$ Tregs in the tumors of vehicle and JQ1/anti–PD-1-treated KP mice. **E,** Percentage of KLRG1$^+$ Tregs in the tumors of KP mice as a function of survival time in days. Data in **D** are mean ± SEM for 4–5 mice/group. *, $P < 0.05$; **, $P < 0.01$.

Discussion

Although multiple strategies have been under development against KRAS-mutant NSCLC, *KRAS* remains an untargetable driver oncogene. Concurrent gene alterations make KRAS-driven lung cancers even more heterogeneous and usually more resistant to treatment. Our present study demonstrates that the immune-enhancing properties of agents that disrupt the activity of epigenetics-regulating bromodomain proteins could be harnessed to enhance the therapeutic benefits of immune checkpoint blockade in NSCLC.

Previously, we reported that inhibition of BET bromodomain proteins by JQ1 promoted downregulation of Foxp3 and CTLA-4 in lung tumor-infiltrating Tregs and disrupted their suppressive function (18). Our finding that Treg numbers declined in the presence of JQ1 treatment with or without PD-1 blockade, in the present study, is consistent with this observation, as these signature proteins are crucial for Treg maintenance and survival (34, 35). Whether JQ1 preferentially targets a subpopulation of tumor-infiltrating Tregs warrants further investigation, although our finding that the KLRG1$^+$ Treg subset was diminished with this treatment supports this possibility and the idea that the prevalence of this subset may be associated with tumor severity. As their frequency correlates with tumor burden, we deduce that their increasing proportions is likely causative, rather than a consequence of tumor growth. We surmise that the activated status of this KLRG1$^+$ subset relative to the KLRG1$^-$ cells may be a key feature rendering them more vulnerable to epigenetic modulation, including propensity toward cell death as observed under JQ1 treatment. Their reduced presence under this treatment therefore likely emanates from a gradual disruption in molecular programming that is normally operative in Treg maintenance, which is supported by the more dramatic downregulation of key Treg signature proteins in this subset upon JQ1 administration. Although it is tempting to also speculate that the functions of tumor-associated Tregs may be partially impaired following PD-1 blockade, our data do not provide evidence in support of this. Besides, the role of PD-1 in Treg function remains to be deduced, as indicated by evidence from conflicting reports (36, 37).

Cytokines regulate T-cell differentiation and function (38, 39). The substantially elevated levels of IL12/IFNγ, compared with IL4, IL6, IL10, and IL13, in the presence of JQ1 and anti–PD-1 therapy support the premise that this combination likely promotes Th1 cell differentiation and the observed Th1 cytokines, which are implicated in antitumor immunity (40–42). Future work is planned to interrogate additional conundrums, such as the status

Published OnlineFirst August 7, 2018; DOI: 10.1158/2326-6066.CIR-18-0077

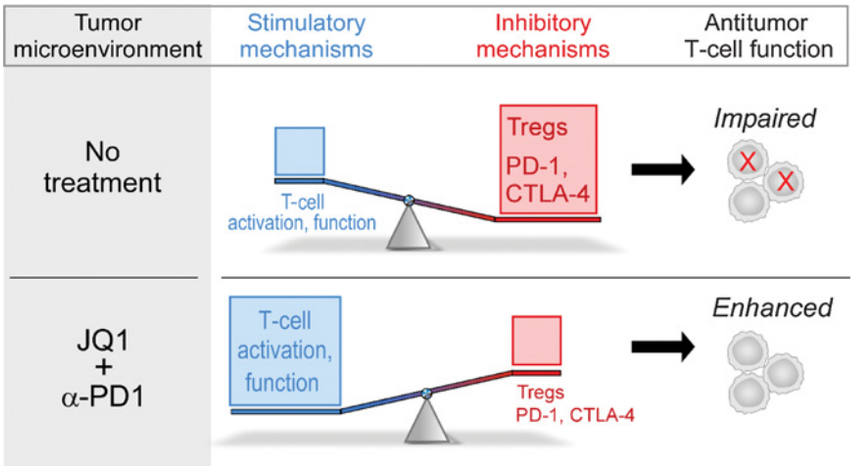

Figure 6.
Proposed model for JQ1/α-PD-1 therapeutic effects in the KP model of NSCLC. In the absence of therapeutic intervention, inhibitory mechanisms including increased Treg presence and PD-1/CTLA-4 expression on tumor-infiltrating T cells outweigh stimulatory mechanisms leading to impairment in antitumor T-cell function. Treatment with JQ1 and α-PD-1 cooperatively reduces these inhibitory mechanisms in distinct ways to allow stimulatory signals to prevail and tip the scale in favor of enhanced T-cell function.

of macrophages recruited to the tumors in the presence of this drug combination (i.e., M1 or M2), which may explain potential sources of these T-cell differentiation–modulating cytokines. Nonetheless, the enhanced activation and improved effector activity of tumor-infiltrating T cells, coupled with a Th1 cytokine profile, all of which were significantly potentiated with the combination treatment, aligns well with the durable antitumor response seen with this novel therapy combination.

A number of reports demonstrate that BET bromodomain proteins regulate PD-L1, and their inhibition by JQ1 downmodulates its expression (43–45). Thus, one could argue that the therapeutic effect of JQ1 as shown in this study emanates from this effect on PD-L1. Our findings do not support this premise, as we found only a modest decrease in PD-L1 expression on TAMs, whereas PD-1 expression was predominantly affected in tumor-infiltrating T cells. This result is consistent with the idea that the therapeutic efficacy of JQ1 in this model can be attributed mostly to its Treg-disruptive effect along with PD1 downregulation in potential effector T cells. We emphasize that JQ1-mediated reduction in PD-1 levels is only partial on conventional T cells, raising the possibility that the residual PD-1–mediated negative signals may contribute to impediment of antitumor responses. Further blocking of remaining PD-1 promotes a more sustained delay of tumor growth. This is consistent with the notion that aggressive attenuation of negative signals induced by this inhibitory axis through a multipronged approach is projected to support enhanced antitumor immunity.

The cooperative nature of both drugs likely stems from a number of plausible arguments. The increased activation profile and effector function associated with JQ1 treatment could be attributed in part to a reduction in tumor-Treg proportions, which are reported to inhibit T-cell activation, proliferation, and effector function in various inflammatory settings (34). The reduced levels of molecular checkpoints, such as PD-1 on tumor-associated conventional T cells, is another plausible explanation for these phenotypic changes upon JQ1 treatment. Engagement of these inhibitory receptors blunt T-cell priming, a series of events that include T-cell activation (46–48). In the case of PD-1 blockade, a reinvigoration of partially exhausted tumor T cells is one of the likely mechanisms accounting for the enhancement in T-cell effector function as demonstrated by *ex vivo* functional studies. Thus, we believe the mechanism for the cooperative effect between JQ1 and anti–PD-1 in the present study is a multifaceted targeting of inhibitory signals in the tumor microenvironment: JQ1-mediated reduction of Tregs, especially a highly suppressive KLRG1$^+$ subset, and the dampening of the negative TCR signaling that is normally operative in the presence of unperturbed PD-1–PD-L1 signaling.

The idea that JQ1 promotes a reduction in PD-1 expression on tumor-CD8$^+$ T cells, whereas anti–PD-1 blocks residual PD-1 signaling, is an attractive one for immunotherapy design, as existing reports demonstrate only a subset of patients derive therapeutic benefits from anti–PD-1 therapy. Our data highlight the notion that tumor immunity is a balancing act (Fig. 6), in which inhibitory mechanisms must be reversed or attenuated sufficiently to allow stimulatory mechanisms to prevail. This notion is supported by the finding that the most robust effector activity by tumor CD8$^+$ T cells (as measured by IFNγ secretion) coincided with the lowest proportion of PD-1–expressing cells. This introduces the possibility that the differential responses to anti–PD-1 therapy observed in the clinic is a reflection of the degree of success to which PD-1 signals are dampened in patients. As more data emerge from clinical use of anti–PD-1 therapy, this hypothesis may be supported if pretreatment PD-1 levels correlate with therapeutic response to anti–PD-1 therapy. Nevertheless, targeting inhibitory immune checkpoint receptors on multiple fronts in addition to dampening suppressive T-cell presence, as was done here with BET bromodomain inhibition and PD-1 blockade, promotes a tumor-immune microenvironment whereby potential tumor-reactive T cells can better exert their antitumor functions with less impedance.

We hereby propose that BET inhibitors such as JQ1 are a double-edged sword that will likely complement the therapeutic efficacy of immune checkpoint blockade. On the one hand, they evoke tumor cell–intrinsic effects, such as changes in the transcriptional landscape characterized by downregulation of genes encoding tumor growth and survival proteins, as well as concurrent upregulation of a number of tumor suppressors. On the other hand, their immunostimulatory effect is projected to favor increased immune reactivity in tumor settings. Despite JQ1's antiproliferative effect on tumor cells (15–17, 49), the long-lasting therapeutic outcomes following treatment with JQ1 or when coupled with anti–PD-1 therapy seen in the present study

Published OnlineFirst August 7, 2018; DOI: 10.1158/2326-6066.CIR-18-0077

was not reproduced in immunodeficient mice treated with either drug, suggesting that immune (T) cells predominantly contribute to the antitumor benefits derived from this dual-agent treatment regimen. The possibility that JQ1 may have deleterious effects on non-Tregs, i.e., potential effector T cells, in humans is a point of consideration; however, in the present study, we found that mice tolerated the combination quite well. There was also no evidence for deleterious or toxic effects of JQ1/anti–PD-1 on T conventional cells *in vitro*, suggesting a relatively safe profile in the context of tumor-associated T cells.

With PD-1–blocking antibodies already approved by the FDA for management of advanced/metastatic lung cancer, and JQ1-like drugs in clinical testing, our proof-of-concept study demonstrates promising therapeutic efficacy by combining these drugs to improve antitumor responses that exceed the potential of either agent alone. As immunotherapeutic agents evolve beyond prototypical agents such as antibodies, rationally selected combinatorial approaches, such as the approach taken in this study, warrant further investigation and future evaluation in the clinic.

Disclosure of Potential Conflicts of Interest

J.E. Bradner is president at Novartis Institutes for BioMedical Research and has ownership interest (including stock, patents, etc.) in Novartis. A. Tsirigos is a consultant/advisory board member for Intelligencia. G.J. Freeman has ownership interest (including stock, patents, etc.) in Roche, Merck, Bristol-Myers Squibb, EMD Serono, Boehriner Ingelheim, AstraZeneca, Novartis, and Dako. H. Chen has ownership interest (including stock, patents, etc.) in AstraZeneca. No potential conflicts of interest were disclosed by the other authors.

Authors' Contributions

Conception and design: D.O. Adeegbe, S. Liu, J.E. Bradner, H. Chen, K.-K. Wong
Development of methodology: D.O. Adeegbe, S. Liu, M. Bowden, C.W. Zhou, M. Grondine, E.V. Ivanova, G.J. Freeman, K.-K. Wong
Acquisition of data (provided animals, acquired and managed patients, provided facilities, etc.): D.O. Adeegbe, S. Liu, M.M. Hattersley, M. Bowden, C.W. Zhou, S. Li, R. Vlahos, M. Grondine, E.V. Ivanova, M.M. Quinn, P. Gao, K.-K. Wong
Analysis and interpretation of data (e.g., statistical analysis, biostatistics, computational analysis): D.O. Adeegbe, S. Liu, M.M. Hattersley, M. Bowden, R. Vlahos, M. Grondine, I. Dolgalev, E.V. Ivanova, A.K. Rustgi, K.-K. Wong
Writing, review, and/or revision of the manuscript: D.O. Adeegbe, S. Liu, M.M. Hattersley, S. Li, P.S. Hammerman, A.K. Rustgi, A.J. Bass, G.J. Freeman, H. Chen, K.-K. Wong
Administrative, technical, or material support (i.e., reporting or organizing data, constructing databases): D.O. Adeegbe, C.W. Zhou, I. Dolgalev, P.S. Hammerman, J.E. Bradner, J.A. Diehl, G.J. Freeman
Study supervision: D.O. Adeegbe, P.S. Hammerman, H. Chen
Other (bioinformatics supervision): A. Tsirigos

Acknowledgments

The authors would like to thank Zach Herbert (Dana-Farber Molecular Biology Core Facility) for RNA-seq and data assistance and Ting Chen and Yanxi Zhang for technical assistance. This work was supported by NCI R01 CA216188, CA205150, CA166480, CA213333, CA098101, and CA154303 to K.K. Wong.

The costs of publication of this article were defrayed in part by the payment of page charges. This article must therefore be hereby marked *advertisement* in accordance with 18 U.S.C. Section 1734 solely to indicate this fact.

Received February 9, 2018; revised May 22, 2018; accepted August 2, 2018; published first August 7, 2018.

References

1. Swanton C, Govindan R. Clinical implications of genomic discoveries in lung cancer. N Engl J Med 2016;374:1864–73.
2. Comprehensive molecular profiling of lung adenocarcinoma. Nature 2014;511:543–50.
3. Roberts PJ, Stinchcombe TE. KRAS mutation: should we test for it, and does it matter? J Clin Oncol 2013;31:1112–21.
4. Chen Z, Cheng K, Walton Z, Wang Y, Ebi H, Shimamura T, et al. A murine lung cancer co-clinical trial identifies genetic modifiers of therapeutic response. Nature 2012;483:613–7.
5. Skoulidis F, Byers LA, Diao L, Papadimitrakopoulou VA, Tong P, Izzo J, et al. Co-occurring genomic alterations define major subsets of KRAS-mutant lung adenocarcinoma with distinct biology, immune profiles, and therapeutic vulnerabilities. Cancer Discov 2015;5:860–77.
6. Allis CD, Jenuwein T. The molecular hallmarks of epigenetic control. Nat Rev Genet 2016;17:487–500.
7. Liu F, Wang L, Perna F, Nimer SD. Beyond transcription factors: how oncogenic signalling reshapes the epigenetic landscape. Nat Rev Cancer 2016;16:359–72.
8. Ahuja N, Sharma AR, Baylin SB. Epigenetic therapeutics: a new weapon in the war against cancer. Annu Rev Med 2016;67:73–89.
9. Copeland RA, Olhava EJ, Scott MP. Targeting epigenetic enzymes for drug discovery. Curr Opin Chem Biol 2010;14:505–10.
10. Tough DF, Tak PP, Tarakhovsky A, Prinjha RK. Epigenetic drug discovery: breaking through the immune barrier. Nat Rev Drug Discov 2016;15:835–53.
11. Khalil DN, Smith EL, Brentjens RJ, Wolchok JD. The future of cancer treatment: immunomodulation, CARs and combination immunotherapy. Nat Rev Clin Oncol 2016;13:394.
12. Palucka AK, Coussens LM. The basis of oncoimmunology. Cell 2016;164:1233–47.
13. Zuber J, Shi J, Wang E, Rappaport AR, Herrmann H, Sison EA, et al. RNAi screen identifies Brd4 as a therapeutic target in acute myeloid leukaemia. Nature 2011;478:524–8.
14. Filippakopoulos P, Qi J, Picaud S, Shen Y, Smith WB, Fedorov O, et al. Selective inhibition of BET bromodomains. Nature 2010;468:1067–73.
15. Delmore JE, Issa GC, Lemieux ME, Rahl PB, Shi J, Jacobs HM, et al. BET bromodomain inhibition as a therapeutic strategy to target c-Myc. Cell 2011;146:904–17.
16. Puissant A, Frumm SM, Alexe G, Bassil CF, Qi J, Chanthery YH, et al. Targeting MYCN in neuroblastoma by BET bromodomain inhibition. Cancer Discov 2013;3:308–23.
17. Shimamura T, Chen Z, Soucheray M, Carretero J, Kikuchi E, Tchaicha JH, et al. Efficacy of BET bromodomain inhibition in Kras-mutant non-small cell lung cancer. Clin Cancer Res 2013;19:6183–92.
18. Adeegbe D, Liu Y, Lizotte PH, Kamihara Y, Aref AR, Almonte C, et al. Synergistic Immunostimulatory Effects and therapeutic benefit of combined histone deacetylase and bromodomain inhibition in non-small cell lung cancer. Cancer Discov 2017;7:852–67.
19. Sharma P, Allison JP. Immune checkpoint targeting in cancer therapy: toward combination strategies with curative potential. Cell 2015;161:205–14.
20. Chen L, Han X. Anti-PD-1/PD-L1 therapy of human cancer: past, present, and future. J Clin Invest 2015;125:3384–91.
21. Reck M, Rodriguez-Abreu D, Robinson AG, Hui R, Csoszi T, Fulop A, et al. Pembrolizumab versus chemotherapy for PD-L1-positive non-small-cell lung cancer. N Engl J Med 2016;375:1823–33.
22. Langer CJ, Gadgeel SM, Borghaei H, Papadimitrakopoulou VA, Patnaik A, Powell SF, et al. Carboplatin and pemetrexed with or without pembrolizumab for advanced, non-squamous non-small-cell lung cancer: a randomised, phase 2 cohort of the open-label KEYNOTE-021 study. Lancet Oncol 2016;17:1497–508.
23. Zaretsky JM, Garcia-Diaz A, Shin DS, Escuin-Ordinas H, Hugo W, Hu-Lieskovan S, et al. Mutations associated with acquired resistance to PD-1 blockade in melanoma. N Engl J Med 2016;375:819–29.
24. Shin DS, Zaretsky JM, Escuin-Ordinas H, Garcia-Diaz A, Hu-Lieskovan S, Kalbasi A, et al. Primary resistance to PD-1 blockade mediated by JAK1/2 mutations. Cancer Discov 2017;7:188–201.

Published OnlineFirst August 7, 2018; DOI: 10.1158/2326-6066.CIR-18-0077

25. Rizvi NA, Hellmann MD, Snyder A, Kvistborg P, Makarov V, Havel JJ, et al. Cancer immunology. Mutational landscape determines sensitivity to PD-1 blockade in non-small cell lung cancer. Science 2015;348:124–8.
26. Akbay EA, Koyama S, Carretero J, Altabef A, Tchaicha JH, Christensen CL, et al. Activation of the PD-1 pathway contributes to immune escape in EGFR-driven lung tumors. Cancer Discov 2013;3:1355–63.
27. Herter-Sprie GS, Koyama S, Korideck H, Hai J, Deng J, Li YY, et al. Synergy of radiotherapy and PD-1 blockade in Kras-mutant lung cancer. JCI Insight 2016;1:e87415.
28. Kilkenny C, Browne WJ, Cuthill IC, Emerson M, Altman DG. Improving bioscience research reporting: The ARRIVE guidelines for reporting animal research. J Pharmacol Pharmacother 2010;1:94–9.
29. Love MI, Huber W, Anders S. Moderated estimation of fold change and dispersion for RNA-seq data with DESeq2. Genome Biol 2014; 15:550.
30. Peng D, Kryczek I, Nagarsheth N, Zhao L, Wei S, Wang W, et al. Epigenetic silencing of TH1-type chemokines shapes tumour immunity and immunotherapy. Nature 2015;527:249–53.
31. Quail DF, Joyce JA. Microenvironmental regulation of tumor progression and metastasis. Nat Med 2013;19:1423–37.
32. Whiteside TL. The tumor microenvironment and its role in promoting tumor growth. Oncogene 2008;27:5904–12.
33. Bin Dhuban K, Kornete M, Mason ES, Piccirillo CA. Functional dynamics of Foxp3(+) regulatory T cells in mice and humans. Immunol Rev 2014;259:140–58.
34. Ohkura N, Kitagawa Y, Sakaguchi S. Development and maintenance of regulatory T cells. Immunity 2013;38:414–23.
35. Friedline RH, Brown DS, Nguyen H, Kornfeld H, Lee J, Zhang Y, et al. CD4+ regulatory T cells require CTLA-4 for the maintenance of systemic tolerance. J Exp Med 2009;206:421–34.
36. Zhang B, Chikuma S, Hori S, Fagarasan S, Honjo T. Nonoverlapping roles of PD-1 and FoxP3 in maintaining immune tolerance in a novel autoimmune pancreatitis mouse model. Proc Natl Acad Sci U S A 2016;113: 8490–5.
37. Penaloza-MacMaster P, Kamphorst AO, Wieland A, Araki K, Iyer SS, West EE, et al. Interplay between regulatory T cells and PD-1 in modulating T cell exhaustion and viral control during chronic LCMV infection. J Exp Med 2014;211:1905–18.
38. Zhu J, Yamane H, Paul WE. Differentiation of effector CD4 T cell populations. Annu Rev Immunol 2010;28:445–89.
39. Cox MA, Harrington LE, Zajac AJ. Cytokines and the inception of CD8 T cell responses. Trends Immunol 2011;32:180–6.
40. Tugues S, Burkhard SH, Ohs I, Vrohlings M, Nussbaum K, Vom Berg J, et al. New insights into IL-12-mediated tumor suppression. Cell Death Differ 2015;22:237–46.
41. Disis ML. Immune regulation of cancer. J Clin Oncol 2010;28:4531–8.
42. Zanetti M.Tapping CD4 T cells for cancer immunotherapy: the choice of personalized genomics. J Immunol 2015;194:2049–56.
43. Zhu H, Bengsch F, Svoronos N, Rutkowski MR, Bitler BG, Allegrezza MJ, et al. BET Bromodomain inhibition promotes antitumor immunity by suppressing PD-L1 expression. Cell Rep 2016;16:2829–37.
44. Melaiu O, Mina M, Chierici M, Boldrini R, Jurman G, Romania P, et al. PD-L1 is a therapeutic target of the bromodomain inhibitor JQ1 and, combined with HLA class I, a promising prognostic biomarker in neuroblastoma. Clin Cancer Res 2017;23:4462–72.
45. Hogg SJ, Vervoort SJ, Deswal S, Ott CJ, Li J, Cluse LA, et al. BET-Bromodomain inhibitors engage the host immune system and regulate expression of the immune checkpoint ligand PD-L1. Cell Rep 2017;18:2162–74.
46. Boussiotis VA. Molecular and biochemical aspects of the PD-1 checkpoint pathway. N Engl J Med 2016;375:1767–78.
47. Rudd CE, Taylor A, Schneider H. CD28 and CTLA-4 coreceptor expression and signal transduction. Immunol Rev 2009;229:12–26.
48. Wei SC, Levine JH, Cogdill AP, Zhao Y, Anang NAS, Andrews MC, et al. Distinct cellular mechanisms underlie anti-CTLA-4 and anti-PD-1 checkpoint blockade. Cell 2017;170:1120–33.
49. Bhadury J, Nilsson LM, Muralidharan SV, Green LC, Li Z, Gesner EM, et al. BET and HDAC inhibitors induce similar genes and biological effects and synergize to kill in Myc-induced murine lymphoma. Proc Natl Acad Sci U S A 2014;111:E2721–30.

Published OnlineFirst August 7, 2018; DOI: 10.1158/2326-6066.CIR-18-0077

Cancer Immunology Research

BET Bromodomain Inhibition Cooperates with PD-1 Blockade to Facilitate Antitumor Response in *Kras*-Mutant Non–Small Cell Lung Cancer

Dennis O. Adeegbe, Shengwu Liu, Maureen M. Hattersley, et al.

Cancer Immunol Res 2018;6:1234-1245. Published OnlineFirst August 7, 2018.